Contrib Mineral Petrol
DOI 10.1007/s00410-011-0633-4

ORIGINAL PAPER

The origin of high-Mg magmas in Mt Shasta and Medicine Lake volcanoes, Cascade Arc (California): higher and lower than mantle oxygen isotope signatures attributed to current and past subduction

E. Martin · I. Bindeman · T. L. Grove

Received: 12 October 2009 / Accepted: 25 March 2011

Abstract We report the oxygen isotope composition of olivine and orthopyroxene phenocrysts in lavas from the main magma types at Mt Shasta and Medicine Lake Volcanoes: primitive high-alumina olivine tholeiite (HAOT), basaltic andesites (BA), primitive magnesian andesites (PMA), and dacites. The most primitive HAOT (MgO > 9 wt%) from Mt. Shasta has olivine $\delta^{18}O$ ($\delta^{18}O_{Ol}$) values of 5.9–6.1‰, which are about 1‰ higher than those observed in olivine from normal mantle-derived magmas. In contrast, HAOT lavas from Medicine Lake have $\delta^{18}O_{Ol}$ values ranging from 4.7 to 5.5‰, which are similar to or lower than values for olivine in equilibrium with mantle-derived magmas. Other magma types from both volcanoes show intermediate $\delta^{18}O_{Ol}$ values. The oxygen isotope composition of the most magnesian lavas cannot be explained by crustal contamination and the trace element composition of olivine phenocrysts precludes a pyroxenitic mantle source. Therefore, the high and variable $\delta^{18}O_{Ol}$ signature of the most magnesian samples studied (HAOT and BA) comes from the peridotitic mantle wedge itself. As HAOT magma is generated by anhydrous adiabatic partial melting of the shallow mantle, its 1.4‰ range in $\delta^{18}O_{Ol}$ reflects a heterogeneous composition of the shallow mantle source that has been influenced by subduction fluids and/or melts sometime in the past. Magmas generated in the mantle wedge by flux melting due to modern subduction fluids, as exemplified by BA and probably PMA, display more homogeneous composition with only 0.5‰ variation. The high-$\delta^{18}O$ values observed in magnesian lavas, and principally in the HAOT, are difficult to explain by a single-stage flux-melting process in the mantle wedge above the modern subduction zone and require a mantle source enriched in ^{18}O. It is here explained by flow of older, pre-enriched portions of the mantle through the slab window beneath the South Cascades.

Keywords Cascades · Oxygen isotopes · Subduction · Mantle wedge · Flux melting

Communicated by J. Hoefs.

Electronic supplementary material The online version of this article (doi:10.1007/s00410-011-0633-4) contains supplementary material, which is available to authorized users.

E. Martin · I. Bindeman
Department of Geological Sciences, University of Oregon, Eugene, OR 97403-1272, USA

E. Martin (✉)
Institut des sciences de la Terre de Paris (ISTeP), UMR 7193 CNRS-UPMC (Paris VI), 75005 Paris, France
e-mail: erwan.martin@upmc.fr

T. L. Grove
Department of Earth, Atmospheric and Planetary Sciences, Massachusetts Institute of Technology, Cambridge, MA 02139, USA

Introduction

Magmas from convergent margins exhibit large compositional variability due to the effects of fractional crystallization, crustal assimilation, and derivation from various sources in the slab, mantle wedge, and crust. The main process that leads to the generation of primitive arc basalts and new arc crust is the melting of the peridotitic mantle wedge due to the fluxing of hydrous fluids derived from the subducted slab (e.g., Stolper and Newman 1994). It has been suggested that high fluid fluxing through the mantle wedge leads to the formation of high-Mg basaltic andesite and andesites rather than basalts (e.g., Grove et al. 2002);

Published online: 20 April 2011

thus, the genesis of high-Mg basaltic andesite and andesite in arc settings may provide the key to our understanding of flux-induced melting in the mantle. Furthermore, while most researchers consider that the majority of primary arc magmas have basaltic composition; high-Mg andesite is also of importance (e.g., Kelemen 1995). High-Mg andesite has been described in a variety of arc settings (e.g., Kay 1978; Tatsumi 1981, 1982; Tatsumi and Ishizaka 1982; Kay et al. 1982; Smith and Compston 1982; Yogodzinski et al. 1994; Grove et al. 2002; Heyworth et al. 2007; Wood and Turner 2009) and is often attributed to a more hydrous mantle source than for arc basalt magmas (e.g., Hirose 1997; Grove et al. 2006).

Grove et al. (2002) suggested that the subduction-related H_2O-rich fluid component beneath Mt. Shasta has high $Na_2O + K_2O$, low SiO_2, and trace element characteristics that resemble a melt resulting from low degree partial melting of an eclogite. It is likely that this H_2O-rich fluid component (either melt or fluid) reacted with the mantle wedge above the slab and changed its composition. Based on radiogenic isotopes (Sr, Nd, and Pb), Grove et al. (2002) also showed that two fluid components are required. Both of them would come from subducted slab: one from the basaltic crust, the other from the sediments. Ratios of fluid-mobile vs. immobile elements such as Ba/Ce, La/Sm, Sr/Y are useful for tracing and quantifying the subduction fluid contribution in magma genesis. For instance, these tracers, via an increase of their ratios, indicate an increase in the fluid flux from the subducted slab beneath the South Cascades compared with the rest of the volcanic arc (e.g., Bacon et al. 1997; Schmidt et al. 2008).

This study uses oxygen isotopes in order to provide an additional line of evidence for tracing and quantifying the subduction fluid or melt contribution during the genesis of primitive magma. Indeed, the oxygen isotope composition of fluids or melts released from isotopically stratified subducted slab ($\delta^{18}O$ decreasing from $\sim$15 to $\sim$0‰ with depth; e.g., Muehlenbachs 1986) is expected to impart distinctive signatures from the slab. As a consequence, the $\delta^{18}O$ value of mantle-derived magma that is affected by subduction fluids could be significantly different from that of the "normal" mantle-derived magma, which is 5.7 ± 0.2‰ (e.g., Eiler 2001). Consequently, it is expected that the subduction fluid sources can potentially be identified by O-isotope analyses of primitive arc lavas. However, in relatively low fluid/rock ratio systems, the oxygen isotope balance is primarily controlled by the rock and not the fluids. This means that oxygen isotopes can be useful for tracing and quantifying the contribution of subduction fluids in arc magma genesis, especially in locations where the overall fluid/rock ratio has been unusually high.

The Cascades arc shows rather limited range in $\delta^{18}O$ values of olivine ($\delta^{18}O_{Ol} = 5.1 - 5.6$‰; e.g., Ruscitto et al. 2010a). In the south Cascades, however, the few existing whole-rock and phenocryst data for Mt. Shasta (Bacon et al. 1997) and Medicine Lake Volcano lavas (Adami et al. 1996; Bacon et al. 1997; Donnelly-Nolan 1998) demonstrate respectively higher and lower $\delta^{18}O$ compared to the mantle-derived magma value. However, whole-rock and feldspar phenocrysts are susceptible to alteration and cannot always be used as a proxy for magma $\delta^{18}O$ values ($\delta^{18}O_{melt}$).

In this study, we present oxygen isotopes analyses of the most magnesian phenocrysts (olivine and orthopyroxene having Mg# $\sim$ 90%) from the most primitive lavas (MgO $\geq$ 8–9wt.%) of a representative lava suite from Mt. Shasta and Medicine Lake volcanoes. This way it is expected to assess the most primitive $\delta^{18}O_{melt}$, which has not been affected by late contamination and alteration processes. In few samples and in particular those from the S17 locality (see below), "xenocrystic" contamination has been suggested from petrographic arguments and is still at the heart of an active debate (Streck et al. 2007). Nevertheless, here we demonstrate that the measured $\delta^{18}O$ values reflect mantle signatures rather than xenocrystic contamination. We infer that these mantle-equilibrated magmas from the South Cascades provide a better understanding to the overall oxygen-isotope compositions of mantle wedge and subduction fluids as well as the behavior of the latter during slab dehydration.

Geological setting

Located in Northern California, Mount Shasta, and Medicine Lake Volcano represent the cross-arc segment of the southern Cascade subduction zone that spans 55 km (Fig. 1). Mt Shasta is the largest volcano of the Cascades volcanic front, and the large Medicine lake is one of the few rear-arc shield volcanoes (Donnelly-Nolan et al. 2008).

Cascades volcanism is the result of the subduction of the young ($\sim$12–14 Ma) and hot Juan de Fuca and Gorda plates, each with relatively thin sediment cover. Subduction under Mt. Shasta and Medicine Lake volcano is additionally characterized by the presence of the Blanco fracture zone (Fig. 1). The oceanic lithosphere, which is being subducted at a rate of $\sim$4 cm/year (e.g., Wilson 1988) is estimated to be $\sim$110 km beneath Mt. Shasta and $\sim$200 km beneath Medicine Lake (Zucca et al. 1986; Harris et al. 1991; Benz et al. 1992).

Mt. Shasta is a stratovolcano which had four stages of cone development: Sargents Ridge (<250–130 ka), Misery Hill (80–10 ka), Shastina (10–9.4 ka), and Hotlum (6–2 ka; Christiansen et al. 1977). Spatially and temporally associated with the satellite cones, the lava suite consists of high-alumina olivine tholeiites (HAOT), basaltic andesites

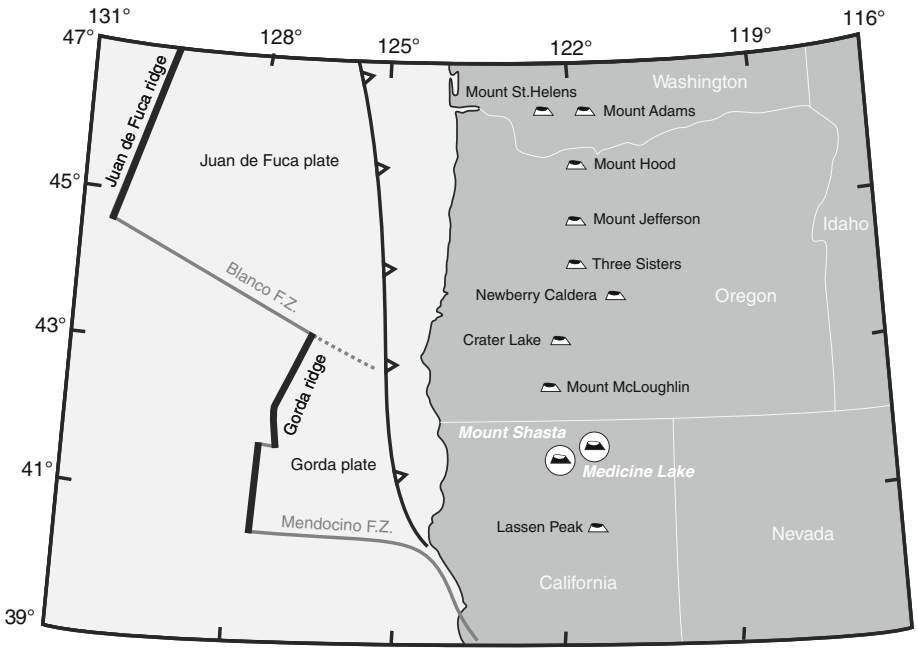

Fig. 1 General tectonic setting of the Cascade volcanic arc showing the Blanco and Mendocino fracture zones, the subduction trench, and principal volcanoes, including Mount Shasta and Medicine Lake Volcano

(BA), primitive magnesian andesites (PMA), andesite, and dacite. The rocks which potentially underlie the volcanic edifice include mainly andesites from the Tertiary Cascade series but also the Trinity ultramafic complex and granitic batholiths of the Jurassic to Cretaceous ages, and finally some sedimentary rocks (e.g., James 2002, Ceuleneer and Le Sueur 2008).

Medicine Lake is a shield volcano that has been built in five major stages from 500 ka to the present (Donnelly-Nolan et al. 2008). The entire lava suite consists of basalt, high-alumina olivine tholeiites (HAOT), basaltic andesites (BA), andesites, dacite, and rhyolite. Almost all lava types have been present throughout the entire Medicine Lake volcano history, with silicic extrusive volcanism dominating before 300 ka and switching to the eruption of hot, anhydrous, predominantly mafic volcanism (HAOT, basalt, and BA) after 300 ka.

Samples and analytical methods

Samples

The suite of Mt. Shasta samples studied (Table 1) represents the most primitive lavas from the Cascades (with respect to MgO contents). The HAOT are nearly aphyric and contain rare, small phenocrysts of olivine and plagioclase (usually $\leq$200 μm). The BA and PMA contain from $<$1 up to 10–15% phenocrysts of olivine and pyroxenes (mainly orthopyroxene). Only in few samples a small amount of plagioclase crystals can be observed. The dacite contains 10–30% phenocrysts with plagioclase as the dominant phase followed by orthopyroxene. As described below (and also by Baker et al. 1994), the olivine and orthopyroxene phenocrysts from the most mafic magmas (HAOT, BA, and PMA) are homogeneous in composition or display subtle normal zoning. However, some orthopyroxene phenocrysts in dacite and in a few selected PMA samples show reverse zoning and has been interpreted as resulting from magma mixing (e.g., Streck et al. 2007).

Samples from Medicine Lake volcano studied in this paper are listed in Table 2 and consist of HAOT and BA. These rocks are nearly aphyric with $<$4% phenocrysts of plagioclase, small ($\leq$100 μm) olivine, and rare pyroxene.

For Mt. Shasta, O-isotopes in olivine and orthopyroxene crystals were measured both on the same samples previously studied by Anderson (1973, 1974a, b, 1976, 1979), Baker et al. (1994), Grove et al. (2002) and our personal collection from the same field localities described by these authors (see Table 1, 2 and Supplementary material 1). For the Medicine Lake samples, we analyzed O-isotope compositions of olivine from lavas that we collected ourselves from the same units and same location as the samples studied by Adami et al. (1996), Bacon et al. (1997), Donnelly-Nolan (1998), Kinzler et al. (2000) and Donnelly-Nolan et al. (2008; Table 2). Most samples from this study were already characterized for their major and trace elements as well as radiogenic isotopic ratios (Supplementary material 2), allowing a direct comparison with oxygen isotopes.

Methods

The oxygen isotope composition of olivine and orthopyroxene phenocrysts was determined by laser fluorination in

Table 1 Oxygen isotope composition of olivine and orthopyroxene phenocrysts and the calculated values of equilibrium melt in the Mt. Shasta lavas and whole-rock composition of serpentinite from the Trinity ultramafic complex

Sample	Lat. 41°	Long. 122°	Rock type	SiO_2	MgO	Mg#	Mineral (*n*)	Max Mg# in mineral's core	$\delta^{18}O_{Ol}$	1 SD	2 SE	$\delta^{18}O_{melt}$
85-51	23.47	1.49	HAOT	48.5	9.2	64.2	Ol (2)	86.2	5.89	0.04	0.06	6.66
85-38	33.54	15.34	HAOT	49.1	9.6	66.5	Ol (3)		6.08	0.15	0.17	6.85
95-15	20.85	10.03	BA	50.9	10.7	72.1	Ol (2)	90.6	5.38	0.01	0.01	6.31
85-44	28.64	17.97	BA	51.2	10.7	70.8	Ol (2)	90.2	5.65	0.01	0.02	6.58
85-1a	32.65	16.78	BA	51.5	10.6	71.4	Ol (3)	90.4	5.55	0.07	0.08	6.48
97-2	19.15	10.07	BA	51.9	9.4	70.6	Ol (2)	90.9	5.61	0.05	0.07	6.54
95-17	19.2	10	BA	51.3	8.4	65.9	Ol (2)	84.4	5.44	0.05	0.08	6.37
85-48c	22.11	12.48	BA	53.6	8.3	67.6	Opx (2)	87.8	5.31	0.01	0.02	6.40
82-94a	28.76	11.37	BA	52.5	10.2	72.0	Ol (3)	90.9	5.81	0.23	0.27	6.74
85-41b	34.01	7.88	PMA	57.9	8.9	73.6	Ol (2)–Opx (2)	93.3 (Ol)–84.0 (Opx)	5.43 (Ol)–5.63 (Opx)	0.14	0.14	6.61
S17-1	34.01	7.88	PMA	57.9	8.9	73.6	Opx (2)	87.9	5.85	0.05	0.07	6.90
S17-3	34.01	7.88	PMA	57.9	8.9	73.6	Ol (3)–Opx (3)	87.9 (Ol)–93.1 (Opx)	5.64 (Ol)–5.66 (Opx)	0.16	0.14	6.73
S17-4	34.01	7.88	PMA	57.9	8.9	73.6	Opx (2)	84.6	5.68	0.21	0.29	6.73
S17	34.01	7.88	PMA	58.2	8.5	73.3	Opx (2)	91.4	5.74	0.07	0.09	6.79
97-7	24.48	13.38	D	63.0	3.5	62.1	Opx (3)	89.8	5.82	0.24	0.27	7.39
S76-1	26.22	13.48	D	64.2	3.3	63.2	Opx (2)	87.7	5.63	0.15	0.21	7.20
S76-2	26.22	13.48	D	64.2	3.3	63.2	Opx (3)	86.6	5.74	0.22	0.25	7.31
									$\delta^{18}O_{WR}$			
Trinity 1	15.25	25.35	Serp.				Whole rock (1)		5.37			
Trinity 2	13.97	26.78	Serp.				Whole rock (1)		5.57			

Mineral: *Ol* (olivine) and *Opx* (orthopyroxene), *n* is the number of analyses. The $\delta^{18}O$ values of orthopyroxene are only ~0.42 and ~0.62‰ higher than $\delta^{18}O$ values of olivine at formation temperatures of the BA or PMA (1200°C) and dacite (950°C), respectively (Chiba et al. 1989). Therefore, we subtracted 0.42 to 0.62‰ from measured $\delta^{18}O_{Opx}$ values depending on rock composition and temperature to obtain the calculated $\delta^{18}O_{Ol}$ values for comparison purposes with the olivine-bearing samples. The $\delta^{18}O_{melt}$ was calculated from the $\delta^{18}O_{Ol}$ and $\delta^{18}O_{Opx}$ using the A-factors between olivine (and orthopyroxene) and normative mineral components from Chiba et al. (1989) and melt temperatures from Baker et al. (1994), Elkins-Tanton et al. (2001), and Grove et al. (2002). *Serp* serpentinite from the Trinity ultramafic complex. The SiO_2 and MgO content are from Baker et al. (1994) and Grove et al. (2002), except the S17 sample that come from this study. Mg# is calculated assuming FeO as FeO total. Samples S17 (−1, −3, and −4) and S76 (−1 and −2) described by Anderson (1973, 1974a, b, 1976, 1979) come from the same locality and have similar composition as 85–41b and 95–13 from Grove et al. (2002), respectively. (See the Appendix 1 for the whole composition of these samples)

the Stable Isotope Laboratory at the University of Oregon (e.g., Bindeman 2008). From each crushed rock sample, phenocrysts were handpicked under the microscope and the freshest separate was cleaned up. Crystals with inclusions, surface alteration, and irregular shapes were systematically excluded. For one analysis, 1–2 mg is needed, which corresponds to 1–10 (most commonly 1–4) individual crystals, depending on size. For the most aphyric Medicine Lake lavas, separates consisted of about 20 grains. Between 2 and 5 analyses of each separates were performed in order to have a representative characterization for each rock sample and to check for crystal to crystal variability and sample homogeneity. After laser extraction, the oxygen was purified by being passed through boiling mercury and converted to CO_2 gas. The O-isotope ratios were then analyzed with a Finnigan MAT 253 mass spectrometer and normalized to the Gore Mountain Garnet (GMG, $\delta^{18}O = 5.75‰$) and San Carlos Olivine (SCO, $\delta^{18}O = 5.35‰$) standards. The values of the GMG and SCO standards varied from day to day and were $5.59 \pm 0.06‰$ (2σ; $n = 13$) and $5.08 \pm 0.09‰$, (2σ; $n = 12$), respectively, of the course of the study. Consequently, our measurements were corrected by adding 0.10–0.25‰ to the raw values. Based on repeated analyses of standards, the analytical uncertainties on $\delta^{18}O$ measurements are ≤0.1‰.

Additionally, major and trace element (Ni, Mn, Ca, Cr, Na, K, Al, Ti) analyses of olivine and orthopyroxene phenocryst compositions were performed on a CAMECA SX 100 electron microprobe (EMP) at the University of Oregon. The element concentrations were measured using long counting times of 40–120 s (depending on the

Table 2 Oxygen isotope composition of olivine phenocrysts and the calculated values of equilibrium melt of lavas from the Medicine Lake Volcano

Sample	Lat. 41°	Long. 121°	Same locality as	Rock type	SiO_2	MgO	Mg#	Mineral (*n*)	$\delta^{18}O_{Ol}$	1 SD	2 SE	$\delta^{18}O_{melt}$
08MLV-01	31.83	42.67	41 M	BA	52.8	6.73	67.0	Ol (2)	5.40	0.10	0.15	6.43
08MLV-02	31.71	42.61	41 M	BA	52.8	6.73	67.0	Ol (2)	5.54	0.00	0.00	6.57
08MLV-05	32.82	41.57	1114 M	HAOT	49.3	8.79	65.3	Ol (2)	4.91	0.21	0.30	5.55
08MLV-12	47.08	36.90	767 M	HAOT	47.3	10.4	71.1	Ol (2)	5.25	0.16	0.22	5.89
08MLV-13	47.08	36.90	767 M	HAOT	47.3	10.4	69.1	Ol (2)	5.35	0.19	0.26	5.99
08MLV-14	47.00	34.10	851 M	HAOT	47.6	9.91	68.6	Ol (2)	4.69	0.01	0.01	5.33
08MLV-16	51.23	23.30	640 M	HAOT	48.0	8.52	65.8	Ol (2)	4.94	0.02	0.03	5.58
08MLV-17	50.08	24.17	1552 M	HAOT	48.2	8.57	66.2	Ol (2)	5.17	0.03	0.04	5.81
08MLV-20	44.33	31.53	990 M	HAOT	50.2	8.45	68.2	Ol (2)	5.49	0.05	0.07	6.13
08MLV-25	32.32	9.22	1597 M	HAOT	47.8	8.78	67.6	Ol (2)	5.36	0.07	0.10	6.00
08 MLV-27	30.50	12.67	1798M	HAOT	48.0	8.79	67.1	Ol (2)	5.10	0.10	0.14	5.74
08MLV-28	30.50	12.40	1876 M	HAOT	48.2	8.61	67.3	Ol (2)	5.25	0.04	0.06	5.89
08MLV-30	38.02	21.75	1859 M	HAOT	48.3	9.66	65.7	Ol (2)	4.84	0.21	0.29	5.48

Mineral *Ol* olivine, *n* is the number of analyses. The $\delta^{18}O_{melt}$ was calculated as in Table 1. The SiO_2 and MgO contents are from Adami et al. (1996), Bacon et al.(1997), Donnelly-Nolan (1998), Kinzler et al. (2000), and Donnelly-Nolan et al. (2008) for the same units and localities. Mg# is calculated assuming FeO as FeO total. Medicine Lake volcano high-Mg basalts are olivine poor (<1–2%) with small (<0.5 mm) subphenocryst. Olivine crystals from the most magnesian HAOT and BA from Medicine Lake are classically forsterite 85–90 (Baker et al. 1991; Kinzler et al. 2000) and in Fe–Mg equilibrium with their host rock. (See the Appendix 2 for the whole composition of these samples)

element) to ensure better precision as recommended by Sobolev et al. (2007). The operating conditions were 15 kV and 100 nA for the acceleration voltage and the beam current, respectively, and the spot size was <1 μm. The EMP was calibrated on natural and synthetic mineral standards, and the data were corrected using the improved ZAF or Phi-Rho-Z procedures.

Results

Major and trace element compositions of olivine and orthopyroxene phenocrysts

We studied petrographic features such as zoning patterns in thin sections and by electron microprobe and performed major and trace element analysis of olivine and pyroxene phenocrysts in all Mt. Shasta samples selected for oxygen isotope analysis (Table 1). The forsterite contents (or Mg#) of olivine phenocrysts in magnesian lavas range from 84.4 to 93.3%, with an average of 89.5% (Table 1). The majority of olivine grains show no zoning. Only two grains from the 97-2 sample show an insignificant normal zoning (core to rim) from Fo_{91} to Fo_{89} and from $Fo_{88.5}$ to $Fo_{86.7}$. Major element analyses of host rocks were used to calculate olivine-rock Fe–Mg equilibrium, assuming $K_{D(melt-olivine)} = 0.3 \pm 0.03$ (e.g., Roeder and Emslie 1970). It appears that olivine with forsterite contents between 88 and 93% are in equilibrium with the host magnesian BA and PMA (Mg# > 0.7; Table 1).

Nonetheless, olivine xenocrysts that are large and irregular in shape and have a forsteritic content of 93.3% are present in several samples, including the S17 and 85-41b (Table 1). Our own investigation of this field locality combined with the recent results of Streck et al. (2007) and previous investigations by A.T. Anderson and M. Baker (e.g., Anderson 1976; Baker et al. 1994) confirm <1–2% xenocrystic contamination and the presence of 1–2 mm-size fragments and aggregates of olivine phenocrysts having forsterite content as high as 93.3%. Streck et al. (2007) interpreted these high-Mg# phenocrysts as xenocrysts from the Trinity ultramafic complex but Barr et al. (2007) demonstrated, via the composition of spinel inclusion from the olivine phenocrysts, that these high-Mg# phenocrysts have magmatic compositions and are thus unlikely to be the result of the deserpentinization of the Trinity ultramafic rocks.

The $Fo_{93.3}$ crystals that we analyzed in this study are characterized by homogeneous interior core regions surrounded by thin normally zoned Fe-enriched margins and do not show any re-equilibration textures. We interpret them as antecrysts (crystallized earlier in the same magma). Importantly, during crystal separation, we took care to avoid large and irregular shaped crystals.

Furthermore, the $\delta^{18}O$ measured in the individual olivine phenocrysts from the S-17 locality (sample S17-3) show values between 5.4 and 5.8‰, while the "xenocrysts" have lower $\delta^{18}O$ of 4.9‰ (Table 3) which could be compatible with antecrystic origin. On the other hand, orthopyroxene phenocrysts and "xenocrysts" do not show

Table 3 Oxygen isotope composition of single olivine and orthopyroxene phenocrysts and xenocrysts from S17-3 PMA sample

S17-3		$\delta^{18}O$	Mean $\delta^{18}O$
Olivine	Phenocrysts	5.70	5.64
		5.42	
		5.80	
	Xenocrysts	4.81	4.89
		4.96	
Orthopyroxene	Phenocrysts	6.23	6.08
		5.93	
		6.10	
	Xenocrysts	6.13	6.15
		6.17	

significant differences in their $\delta^{18}O$ values, which are between 5.9 and 6.2‰. Although in S17 samples, the presence (<1–2%) of low-$\delta^{18}O$ "xenocrysts" could explain the greater $\delta^{18}O$ variability between individual olivine crystals compared with other lavas elsewhere, it could not significantly affect the overall $\delta^{18}O$ of the host magma.

Trace element variations in Mt. Shasta olivine phenocrysts reflect the mantle source composition. Given the high magma productivity at Mt Shasta and high $\delta^{18}O$ values of its olivine phenocrysts (see below), we tested whether this could be due to the melting of a fertile mantle source rich in pyroxenite. The approach of Sobolev et al. (2007) allows us to distinguish between pyroxenite versus peridotite sources. Melts and olivine derived from pyroxenite are higher in Ni and Si, but lower in Mn, Ca, and Mg concentrations compared with the peridotite. Our results demonstrate that Mt Shasta olivine phenocrysts plot closer to the peridotitic rather than pyroxenitic field (Fig. 2).

Similar to olivine, the orthopyroxene phenocrysts found in PMA and dacite show high Mg# with an average for maximum value of 88.5. Mg# up to 93.1 is observed in only one orthopyroxene from the PMA sample (S17-3) and is higher than the whole host rock composition equilibrium value, which indicates it could be a xenocryst. Unlike the olivine, pyroxene phenocrysts usually show complex textures and compositional variations with normal, reverse, and patchy zoning; indicating mixing processes (see Streck et al. (2007) for further discussion).

Oxygen isotope composition of olivine and orthopyroxene phenocrysts and melt

Mt. Shasta

Oxygen isotope data for olivine and orthopyroxene phenocrysts from 17 samples are presented in Table 1. The $\delta^{18}O_{Ol}$ values in Mt. Shasta range from 5.31 to 6.08‰

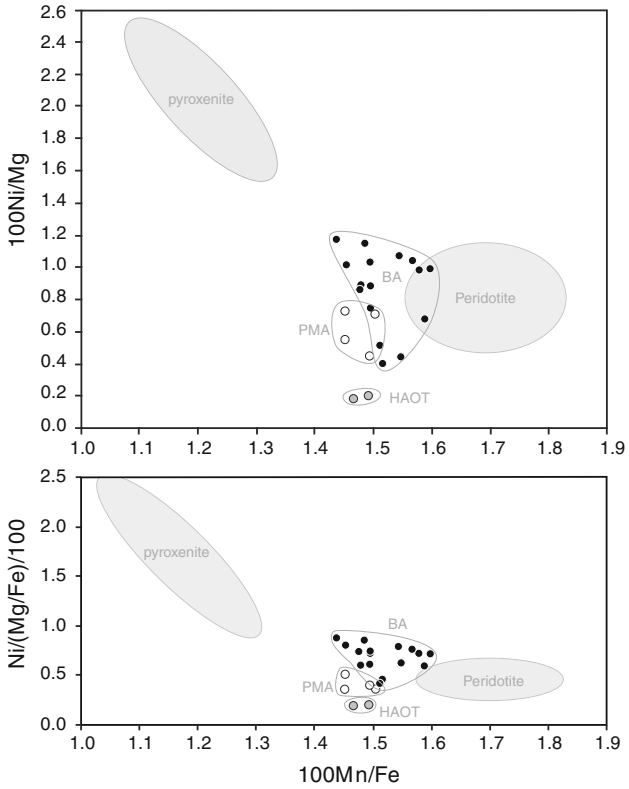

Fig. 2 Trace element compositions of olivine phenocrysts from Mt. Shasta (*circles*) and fields of equilibrium olivine crystals from pyroxenite- and peridotite-derived melts (Sobolev et al. 2007). *HAOT* high-alumina olivine tholeiite, *BA* basaltic andesite, *PMA* primitive magnesian andesite

(Fig. 3), which is up to 1‰ higher than olivine from the normal mantle-derived magmas (5.1 ± 0.2‰, e.g., Eiler 2001). Note that hereafter, high- and low-$\delta^{18}O$ in melt or olivine refer respectively to $\delta^{18}O$ higher and lower than the mantle-derived melt or olivine value (MORB: $\delta^{18}O_{melt}$ = 5.7 ± 0.2‰; $\delta^{18}O_{Ol}$ = 5.1 ± 0.2‰). While HAOTs have the highest $\delta^{18}O_{Ol}$ values (up to 6.08‰), the other lava types (BA, PMA, and dacite) are intermediate between mantle-like and HAOT.

Medicine Lake Volcano

Oxygen isotopes of olivine phenocrysts from 14 primitive samples range from 4.69 to 5.54‰ (Table 2). HAOT accounts for most of these variations and, in contrast to Mt Shasta, shows low to mantle-like $\delta^{18}O_{Ol}$ values (Fig. 3) while BA displays slightly high to mantle-like $\delta^{18}O_{Ol}$ values.

It appears that the HAOTs from Mt Shasta and Medicine Lake volcanoes in the South Cascades segment display a much larger $\delta^{18}O_{Ol}$ range (1.4‰) when compared to arcs worldwide and $\delta^{18}O_{Ol}$ values in other segments of the Cascade arc as shown by our growing database. HAOT

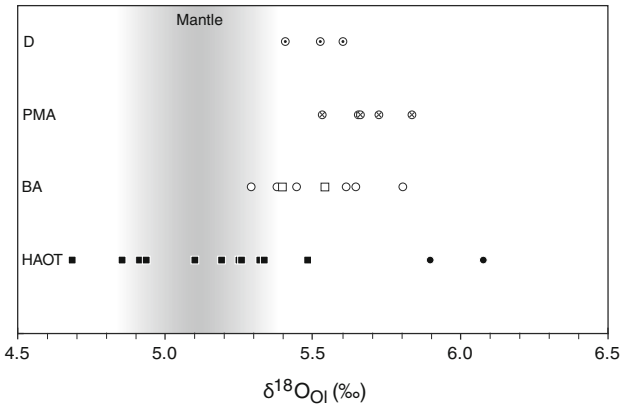

Fig. 3 Oxygen isotope composition of olivine and orthopyroxene crystals from Mt. Shasta (*circles*) and Medicine Lake Volcano (*squares*) lava units (See table 1 for the data). *HAOT* high-alumina olivine tholeiite, *BA* basaltic andesite, *PMA* primitive magnesian andesite, *D* dacite

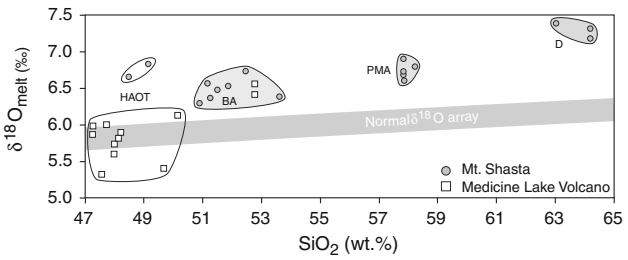

Fig. 4 Calculated $\delta^{18}O_{melt}$ (from the measured $\delta^{18}O_{Ol}$ and $\delta^{18}O_{Opx}$) versus SiO_2 content of the lavas from Mt. Shasta and Medicine Lake Volcano. HAOTs from both volcanoes that reflect the composition of the shallow mantle indicate that this latter is strongly heterogeneous in the South Cascades. However, BAs from both volcanoes have similar composition, which indicates that magmas generated by flux melting have been homogenized in terms of O-isotopes. BA and PMA show a trend that is above but sub-parallel to the "normal $\delta^{18}O$ array" calculated for island arcs (Bindeman et al. 2004), suggesting an initially high-$\delta^{18}O$ source

from Medicine Lake itself has a $\delta^{18}O_{Ol}$ range of 0.8‰, from low- to mantle-like values (Fig. 3), while two samples from Mt Shasta have similarly high $\delta^{18}O_{Ol}$ values with average of 5.99 ± 0.09‰. Lavas of other compositional groups (from both volcanoes) have $\delta^{18}O_{Ol}$ in a 0.5‰ range and plot systematically between the extreme HAOT values observed at both volcanoes: the BA have values of around 5.50‰ while the PMA and dacites have slightly higher values (from 5.54 to 5.84‰; Fig. 3).

In order to calculate melt $\delta^{18}O$ values ($\delta^{18}O_{melt}$) in equilibrium with olivine and orthopyroxene crystals, we performed the following procedure. The $\Delta^{18}O_{Ol\text{-}melt}$ and $\Delta^{18}O_{Opx\text{-}melt}$ fractionation factors in each sample were calculated using the Chiba et al. (1989) method, which takes into account the melt temperatures (estimated for our samples by Baker et al. 1994; Elkins-Tanton et al. 2001; Grove et al. 2002) and CIPW normative compositions (similar to methods outlined in Eiler (2001) and Bindeman et al. (2004)). The calculated $\Delta^{18}O$ are as follow; HAOT: $\Delta^{18}O_{Ol\text{-}melt} = -0.64$ to -0.77‰. BA: $\Delta^{18}O_{Ol\text{-}melt} = -0.93$ to -1.03‰, $\Delta^{18}O_{Opx\text{-}melt} = -0.69$‰. PMA: $\Delta^{18}O_{Ol\text{-}melt} = -1.08$‰, $\Delta^{18}O_{Opx\text{-}melt} = -0.65$‰. Dacite: $\Delta^{18}O_{Opx\text{-}melt} = -1.17$‰, (details are provided in the supplementary material 3). It is noteworthy that in samples from the S17 locality, $\delta^{18}O_{melt}$ independently calculated from olivine and orthopyroxene are comparable (Supplementary material 3), testifying the olivine-orthopyroxene-melt equilibrium. Finally, our calculated $\delta^{18}O_{melt}$ values for each particular sample (Table 1 and 2) are very similar to $\delta^{18}O_{melt}$ values calculated using the Bindeman et al. (2004) method. The latter uses a parameterization of the change in $\Delta^{18}O_{Ol\text{-}melt}$ or $\Delta^{18}O_{Px\text{-}melt}$ with the increase in SiO_2 during the differentiation of average island arc series rocks: $\Delta^{18}O_{Ol\text{-}melt} = 0.88(SiO_2) - 3.57$ and $\Delta^{18}O_{Cpx\text{-}melt} = 0.61(SiO_2) - 2.72$.

We correlated these calculated $\delta^{18}O_{melt}$ values with major, trace, and radiogenic isotope data obtained on whole-rock samples (Supplementary material 1 and 2). When plotted against SiO_2 (Fig. 4), the calculated $\delta^{18}O_{melt}$ values clearly show that the Mt. Shasta lavas (with the exception of the HAOT), describe a trend above, and slightly steeper than the "normal $\delta^{18}O$ array," where the latter corresponds to the fractional crystallization evolution of mantle-derived melt. Primitive lavas from the Medicine Lake volcano display greater scatter for lesser degrees of fractionation (see HAOT compared with BA in Fig. 4).

When plotted against the distance from the trench, $\delta^{18}O_{melt}$ decreases from Mt Shasta to Medicine Lake volcano (Fig. 5). Here, we also plot good tracers of subduction fluid components such as Sr/Y, Li-, and Sr-isotopes, for which the ratios increase with the fluid contribution. It must be noted that the same patterns are observed for other tracers such as La/Sm, Ba/Ce, Ba/Nb, and Pb-isotopes (not plotted here, but see Baker et al. 1994; Bacon et al. 1997; Kinzler et al. 2000; Grove et al. 2002; Donnelly-Nolan et al. 2008). Li isotopic ratios exhibit variations similar to oxygen demonstrating a change from higher (Mt Shasta) to lower than mantle isotopic ratios (Medicine Lake). In both volcanoes, the HAOTs have a lower Sr/Y than in the BAs but still higher than a depleted mantle-derived melt (Sr/Y < 5–10; e.g., Rehkamper and Hofmann 1997). However, all lavas from this study have higher $^{87}Sr/^{86}Sr$ than a depleted mantle-derived melt ($^{87}Sr/^{86}Sr = 0.7025 - 0.7028$; e.g., Rehkamper and Hofmann 1997). Furthermore, the Sr-isotope composition decreases from HAOT to BA lavas in Mt. Shasta area and increases from HAOT to BA in Medicine Lake volcano.

Discussion

Below we discuss the origin of the high $\delta^{18}O$ values found in Mt Shasta's olivine phenocrysts and its relation to the heterogeneous and relatively low $\delta^{18}O$ values measured in those from Medicine Lake volcano. We then consider the relation between these $\delta^{18}O$ signatures and the geodynamic evolution of the subduction zone in the Southern Cascades. Finally, we compare the South Cascades with other subduction zones worldwide where very high $\delta^{18}O$ signatures have recently been measured.

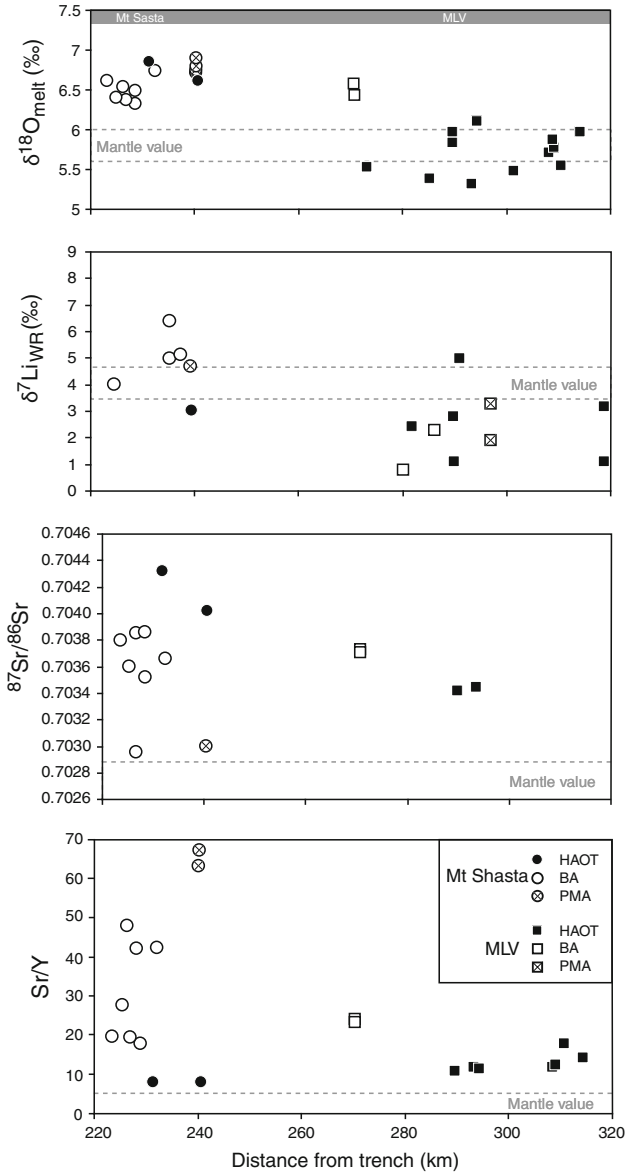

Fig. 5 O-, Li-, and Sr-isotopes and Sr/Y versus distance from the arc trench. Lithium (WR: whole-rock analyses), Strontium isotopes and Sr/Y data are respectively from Magna et al. (2006) and Grove et al. (2002). *MLV* Medicine Lake Volcano

Fractional crystallization

Fractional crystallization and magma mixing played an important role in the petrogenesis of the Mt. Shasta lava suite (e.g., Grove et al. 2005), resulting in a variety of magma types from BA to dacite. However, modeling of the $\delta^{18}O_{melt}$ vs. SiO_2 trend (Fig. 4) demonstrates that a closed system fractionation leads to a 0.3–0.4‰ increase in $\delta^{18}O$ of the siliceous differentiates. Figure 4 shows that the trend described by the BA and PMA of the Mt. Shasta lavas is sub-parallel to the mantle-melt differentiation, which means that the entire range in magma composition (except HAOT; from 51 to 59 wt% SiO_2) can be explained by the fractional crystallization of BA magmas that are initially enriched in ^{18}O. It is noticeable that dacites are about 0.2–0.3‰ higher than the $\delta^{18}O$ expected by the BA–PMA defined differentiation trend. It is most likely that modest crustal contamination occurred during their complex genesis. Considering that crustal contaminants (granitoid-like) have a $\delta^{18}O \sim 10‰$ (e.g., Hoefs 2005 and references therein), a contamination of about 5% can easily explain the observed dacites' enrichment in ^{18}O. Intermediate magma types could also have been generated by mixing between the parental (BA or PMA) and more fractionated magmas (e.g., dacite). Overall, if this differentiation was accompanied by mixing events (mixing with differentiated and less differentiated magma batches of the same line of descent), these episodes will not lead to significant deviation from the $\delta^{18}O_{melt}$–SiO_2 trend. These processes are not relevant for high-Mg and high-$\delta^{18}O$ magmas of this study. We nonetheless discuss the potential effects of the crustal contamination on oxygen isotope composition of the high-Mg magmas from the South Cascades.

Crustal contamination

In the Mt. Shasta and Medicine Lake area, the country rocks are highly diverse in composition and are mostly represented by Mesozoic to Cenozoic volcanic rocks, the Mesozoic Trinity ophiolitic (ultramafic) complex and Mesozoic granitic rocks. To a much lesser extent, some Cenozoic detrital sediments and Paleozoic to Mesozoic metasediments are also present in the area (e.g.. Christiansen et al. 1977; Blakely et al. 1985; Fuis et al. 1987).

Contamination by 5–10% of the Trinity serpentinized peridotite, as suggested by Streck et al. (2007), does not explain the high $\delta^{18}O$ values measured in Mt Shasta olivine crystals. A previous study of the Trinity ophiolite complex (Liakhovitch et al. 2005) reported $\delta^{18}O$ values between 5.3 and 7.5‰ for serpentine polymorph crystals. Here, we measured values of $5.4 \pm 0.1‰$ for two different samples from the Trinity serpentinite (Table 1), whereas O'Leary et al. (1999) reported $\delta^{18}O \sim 4‰$ for whole-rock peridotite and mantle-like values for olivine and clinopyroxene.

All these values are within the range of exposed ultramafic rocks worldwide, which usually have $\delta^{18}O$ values between 3 and 6‰ (e.g., Muehlenbachs 1986). As a consequence, to explain ± 0.5‰ variation of the $\delta^{18}O$ of a mantle-derived magma ($\delta^{18}O_{melt} = 5.8‰$), as observed in the Mt. Shasta and Medicine Lake, more than 40% contamination of the Trinity complex ($3‰ \leq \delta^{18}O \leq 7‰$) is required. Such degree of contamination is unlikely. Furthermore, large olivine crystals with irregular shape from the S17 locality studied here and by Streck et al. (2007) have only marginally lower (not higher) $\delta^{18}O_{Ol}$ values (4.9‰; Table 2) and are thus likely to be antecrysts rather than xenocrysts. The orthopyroxene "xenocrysts" have the same $\delta^{18}O$ than the phenocrysts (Table 2). Therefore, regardless of the degree of xenocrystic contamination, the high-$\delta^{18}O$ signature of Mt Shasta lavas cannot be explained by minor or even moderate addition of the Trinity rocks.

Granitic batholiths in the Southern Cascades have $\delta^{18}O \sim 10‰$ (Masi et al. 1981) and could contribute to the high $\delta^{18}O$ values measured in Mt. Shasta, but it would require a contamination of at least 15–25% of bulk granitic crust ($\delta^{18}O \sim 10‰$). Such voluminous contamination is not realistic: indeed, the high-MgO, high-Ni, and high-Cr contents measured in the most primitive lavas argue against a granitic contamination, which should also lead to higher Rb, Ce, and Zr content (Baker et al. 1994; Grove et al. 2002). Furthermore, as discussed by Magna et al. (2006), the Li- and Sr-isotope compositions preclude more than 5% contamination by a crustal component. If a hypothetical high-$\delta^{18}O$ more mafic crustal component were involved as assimilant (not known in exposed rocks), the amounts of this assimilation mush also have to be very restricted. The last point that makes significant crustal contamination unlikely is that the olivine phenocrysts analyzed in this study have on average a Fo_{89} composition and are in equilibrium with the whole-rock composition and with a peridotitic mantle-derived magma.

The Medicine Lake volcano overlies mostly granitoids (e.g., Lowenstern et al. 2003; Fuis et al. 1987) and the forsterite composition of olivine crystals from the most magnesian HAOT and the BA is typically 85–90% (Baker et al. 1991; Kinzler et al. 2000) and in Fe–Mg equilibrium with their host rock. Therefore, as in the Mt. Shasta case, the isotopic signature measured in olivine from Medicine Lake volcano lavas does not reflect crustal contamination but rather represents the mantle signature.

The origin of heterogeneous $\delta^{18}O$ peridotite-derived melts

Peridotitic or pyroxenitic mantle source?

Pyroxenes in peridotite have ~0.4–0.5‰ higher $\delta^{18}O$ values than coexisting olivine (e.g., Chiba et al. 1989; Mattey et al. 1994). Therefore, a hypothetical pyroxenite source could potentially lead to a melt with respectively higher $\delta^{18}O$ values than a magma having a peridotitic source. However, as illustrated in Fig. 2, trace element concentrations and ratios in analyzed olivine phenocrysts are more consistent with a peridotite-derived than a pyroxenite-derived melt. An additional argument against a pyroxenitic source is that partial melting of pyroxenite leads to relatively low MgO content, in contrast with the high-Mg lavas observed in the Southern Cascades. Therefore, we can also rule out partial melting of a pyroxenitic source as the origin of the high-$\delta^{18}O$ value, and focus below on explaining high and heterogeneous $\delta^{18}O$ in peridotite-derived melts.

O-isotopes composition of subduction fluid component

It is generally accepted that in subduction environments, partial melting of the peridotitic mantle is initiated by the introduction of the slab-derived fluid or melt, which triggers the melting of the mantle wedge (e.g., Gill 1981; Tatsumi et al. 1986; Stolper and Newman 1994; Grove et al. 2002, and many others). These slab-derived fluids or melts equilibrate progressively with the mantle peridotite, transferring the geochemical slab signatures, such as high-$\delta^{18}O$ and high LILE/HFSE, to the mantle wedge.

The components that are capable of imparting a high-$\delta^{18}O$ signature to primitive, mantle-derived magma generated in the mantle wedge are fluids and melts derived from the upper parts of the oceanic crust, and sediments, since in the slab, the $\delta^{18}O$ decreases from ~15 to ~0‰ with depth (e.g., Muehlenbachs 1986). These subduction fluids or melts can achieve a high-$\delta^{18}O$ signature in one of two ways. The first is for the fluid (or melt) to become enriched by a fractionation process between solid and fluid (or melt) during their release from the slab. The second is for the subducted component to already have a high-$\delta^{18}O$ signature when it is released from the slab. Figure 6 illustrates the factors that control enrichment by isotopic fractionation. When the minerals in the subducted slab dehydrate, a fluid is released and its $\delta^{18}O$ value is different than the solid due to isotopic fractionation processes. This isotopic fractionation is expressed as $\Delta^{18}O_{fluid\text{-}rock}$, which is the difference between $\delta^{18}O_{rock}$ and $\delta^{18}O_{fluid}$ and is a function of the temperature. At low temperatures (<300–400°C), $\Delta^{18}O_{fluid\text{-}rock}$ is high meaning that the $\delta^{18}O_{fluid} > \delta^{18}O_{rock}$ ($\Delta^{18}O_{fluid-rock} \geq 10‰$; Fig. 6). At high temperatures (>300–400°C), $\Delta^{18}O_{fluid\text{-}rock}$ is close to 0‰, indicating that the $\delta^{18}O_{fluid} \sim \delta^{18}O_{rock}$. In the South Cascades, the subducting slab is young (12–14 Ma) and "hot," leading to slab dehydration at relatively high temperature beneath the mantle wedge (>400°C for 15 Ma slab; Peacock and Wang 1999). Under such conditions,

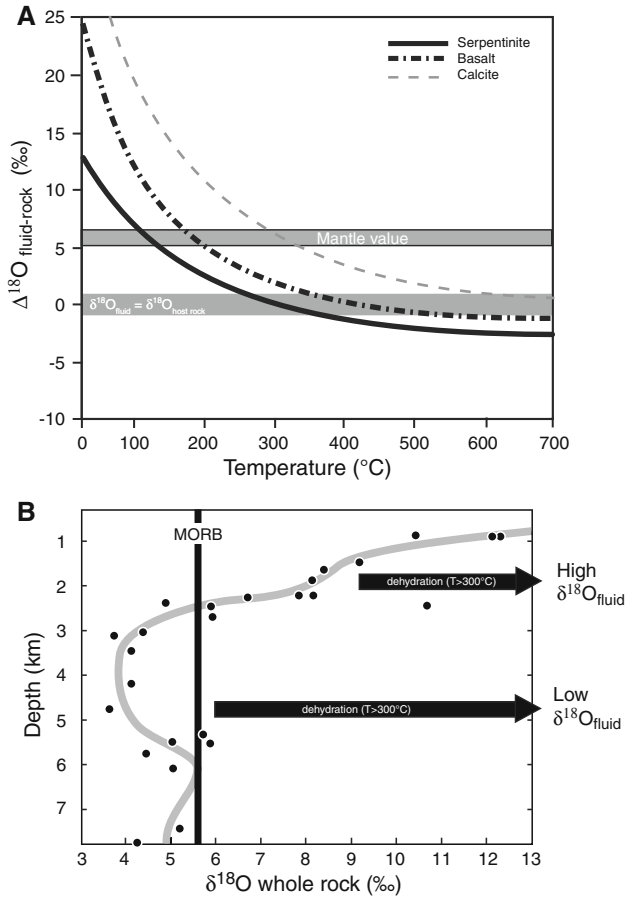

Fig. 6 **a** Relative oxygen isotope fractionation ($\Delta^{18}O_{fluid\text{-}rock}$) between serpentinite, basalt, calcite, and water ($\Delta^{18}O = \delta^{18}O_{rock} - \delta^{18}O_{fluid}$) at different temperatures. Mineral–water isotope fractionations were calculated using Wenner and Taylor (1971), Zheng (1993), and Zhao and Zheng (2003). **b** $\delta^{18}O$ profile in the oceanic crust (modified from Gregory and Taylor 1981). During the oceanic crust evolution, the interaction with seawater ($\delta^{18}O = 0‰$) occurs at temperatures that increase with increasing depth, and led to a global decrease of the lithosphere $\delta^{18}O$ correlative with depth. This led to higher to lower $\delta^{18}O$ values compared with the mantle value (MORB) from the top to the bottom of the oceanic lithosphere. When this latter is subducted, the dehydration beneath the mantle wedge takes place at temperatures higher than 300–400°C. At such temperatures, $\Delta^{18}O$ is close to 0‰, meaning that released fluids have the same composition as the part of the slab that is dehydrating. Therefore, dehydration of the top of the slab leads to high $\delta^{18}O$ fluids and dehydration of the lower part of the slab leads to low $\delta^{18}O$ compared to the mantle value

isotope fractionation is nearly negligible ($\Delta^{18}O_{fluid\text{-}rock} \sim 0$; Fig. 6), meaning that $\delta^{18}O_{fluid}$ values must be comparable to that of the dehydrating part of the slab ($\delta^{18}O_{rock}$). Based on this line of reasoning, fluids released from the shallower portions of the slab (high $\delta^{18}O$ sediment and basalts), will be enriched in ^{18}O (Fig. 6). However, during the course of subduction, the slab heats up as it descends into the mantle, progressively deeper part of the slab dehydrate, and the fluid will then reflect the composition of the deeper portions of the slab (low $\delta^{18}O$ basalt and serpentinite; Fig. 6).

In the following discussion, two regimes of fluid fluxing will be considered: (a) metasomatic and (b) direct fluid-induced melting; with the focus being on their implication for oxygen isotopes and other parameters on Fig. 7. Here, we consider that high-Mg magmas in the South Cascades are generated by 20% partial melting of the mantle wedge (Grove et al. 2002) and this latter have 0.9wt.% water as inferred from the H_2O content measured in olivine-hosted melt inclusions (Anderson 1974b; Ruscitto et al. 2010b; Le Voyer et al. 2010).

In a metasomatic regime, a slab fluid interacts with sufficient amounts of mantle to erase its initial signature (including $\delta^{18}O_{fluid}$). However, if no mantle partial melting occurs, the fluid signature is slowly transferred to the mantle wedge by successive and continuous metasomatic events (e.g., Navon and Stolper 1987). Long-term fluid fluxing of the mantle without partial melting, as in the forearc mantle may variably enrich the mantle wedge with slab-derived fluid signatures, including O-isotopes, and we examine the implications of this process to explain the origin of anhydrous, high-$\delta^{18}O$ HAOT below. In the south Cascades, if the overall fluid/mantle ratio is low (low fluid flux conditions), 0.9–1% of high-$\delta^{18}O$ fluid interacts with 99% of the mantle wedge, and then this metasomatized mantle wedge is partially (20%) melted, scavenging all available water, to generate Mt. Shasta BAs (~4.5wt.% H_2O; Fig. 7). The following fluid types and associated $\delta^{18}O_{fluid}$ values would be required to explain the origin of the hydrous Mt Shasta BAs ($\delta^{18}O_{melt} \sim 6.5‰$). (1) pure water, this model would require $\delta^{18}O_{fluid} \sim 44‰$, (2) water-rich fluid, similar to the one estimated by Grove et al. 2002, (55% water, 35% Na_2O and 10% K_2O), the model requires a subduction component with $\delta^{18}O_{fluid} \sim 31‰$, (3) a hydrous slab melt with 20% H_2O, (e.g., Auer et al. 2009) would need to have $\delta^{18}O_{fluid} \sim 19–21‰$ (see Fig. 7-a for further explanation). Such values exceed the maximum values of the altered oceanic crust and sediment that would be expected to be subducted in the Cascades arc. Only carbonate concretions can reach such high $\delta^{18}O$ values and they are volumetrically insignificant on both the Gorda and Juan de Fuca plates (Goodfellow et al. 1993). We are also not aware of any reports of excessively high CO_2 fluxes under the South Cascades, nor do the melt inclusion data of Ruscitto et al. (2010a, b) or Le Voyer et al. (2010) indicate the presence of elevated CO_2. Using the proposed mass balance calculations and the oxygen isotopes as the evidence, we suggest that a metasomatic regime is not capable of explaining the origin of primitive and hydrous magmas under Mt Shasta.

Under the direct fluid-induced melting conditions, mantle melting proceeds as "flux melting" (Stolper and Newman 1994; Eiler et al. 2000; Grove et al. 2002, 2006) and mantle peridotite dissolves in the ^{18}O-enriched

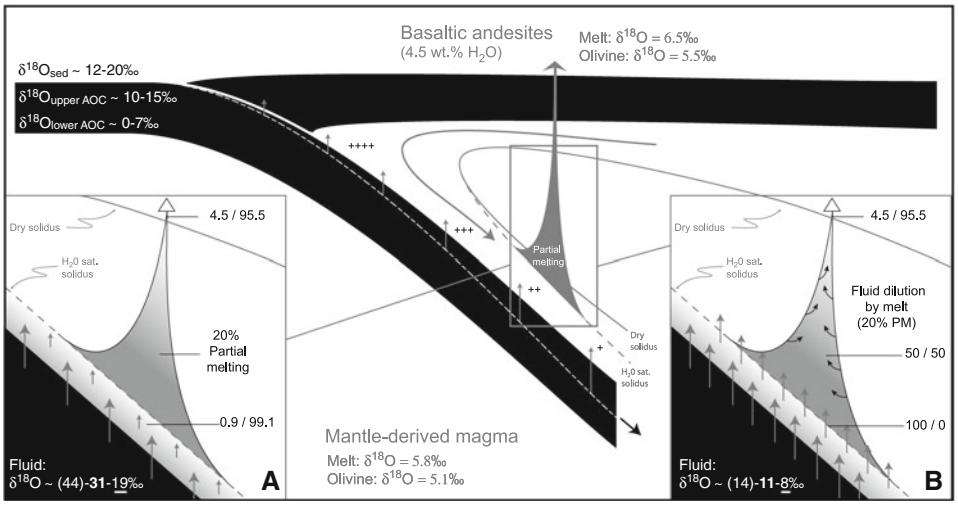

Fig. 7 Schematic figure of the South Cascade subduction zone showing the evolution of the O-isotope composition of melts and fluids during slab dehydration. Sediments and the upper part of the altered oceanic crust (AOC) provide the source of high $\delta^{18}O_{fluid}$ (10–15‰), while the lower part of the slab represents a low $\delta^{18}O_{fluid}$ source (0–7‰; see Fig. 6 and discussion in the text for further explanation). As indicated by the "+", which symbolizes the relative ^{18}O enrichment in fluid, the $\delta^{18}O$ value of the fluids decreases during subduction. This is due to the dehydration of progressively deeper (and lower $\delta^{18}O$) parts of the slab, as shown by the white dashed line. We suggest that this process may explain (at least in part) the lower $\delta^{18}O$ value of the HAOTs from Medicine Lake when compared to those from Mt Shasta. **a** Metasomatic regime: the fluid-rock ratio is low and the mantle wedge is relatively cold so the released fluid reacts and isotopically exchanges with the peridotite before reaching the H_2O-saturated solidus. In order to explain high $\delta^{18}O$ values at Mt Shasta, unrealistically high $\delta^{18}O_{fluid}$ values (19–44‰) are required based on the proportion of mantle melting and fluids known for Mt Shasta. **b** Direct fluid-induced melting regime: the fluid-rock ratio is sufficiently high and conditions are sufficiently hot to cause direct partial flux melting of the mantle wedge, so the high $\delta^{18}O_{fluid}$ slab signature is directly transferred to the melt without being diluted by the large volume of mantle as in the case A. Only this regime can explain the genesis of primitive high-Mg and high-$\delta^{18}O$ magmas from Mt Shasta based on the mass balance calculation. Mass balance calculation: (A) metasomatic regime: 0.9 wt% H_2O is required in the mantle source to generate with 4.5 wt% H_2O magmas by 20% partial melting. Evolution of the "fluid–mantle melt" ratio is indicated in the right end side of the figures A and B. (B) Direct fluid-induced melting regime: fluid dilution by mantle melt requires overall 4.5 wt% H_2O to generate the same amount of water in magmas. $\delta^{18}O_{fluid}$ in parenthesis were calculated considering fluid as pure water, and bold values were estimated considering the Grove et al. (2002) fluid composition (H_2O: 55 wt%, Na_2O: 35 wt%, and K_2O: 10 wt%) and underlined numbers represent the $\delta^{18}O$ of the fluid as an hydrous slab melt (with 20wt.% H_2O) as advocated by Auer et al. (2009) for the Klyuchevskoy volcano. As discussed in the text, the most realistic scenario is a mantle wedge fluxed by water-rich fluid ($\delta^{18}O \sim 11‰$) or by hydrous slab melt ($\delta^{18}O \sim 8‰$), under high fluid-rock ratio conditions (case B)

subduction fluid and/or melt. Therefore, the high-$\delta^{18}O$ slab signatures are instantaneously transferred to the newly formed melt. Under such conditions, Mt. Shasta BAs with $\delta^{18}O_{melt} \sim 6.5‰$ and primary water contents of 4.5wt.%, appear to be the result of mantle fluxing by pure water having $\delta^{18}O_{fluid} \sim 14‰$, a hydrous (55% H_2O) fluid with $\delta^{18}O_{fluid} \sim 11‰$, or a water-rich slab melt with $\delta^{18}O_{fluid} \sim 8‰$ (see Fig. 7 for further explanation). These values are in the range of those from sediment and the upper altered oceanic crust of the front of the Cascades arc (e.g., Goodfellow et al. 1993), and we consider both of these values as realistic for fluids or melts released from subducted sediment or the upper part of the altered oceanic crust.

When compared to subduction $\delta^{18}O_{fluid}$ estimates from other arcs, the slightly elevated $\delta^{18}O_{fluid}$ values that we favor for the South Cascades are comparable to global estimates. For the Tonga-Kermadec arc, where the convergence rate changes from 2 to 20 cm/year, $\delta^{18}O_{melt}$ values of lavas are nearly identical to the normal mantle, suggesting "normal" (MORB-like) subduction $\delta^{18}O_{fluid}$ (Turner et al. 2009). In the Eiler et al. (2005) study of the Central American arc, $\delta^{18}O_{fluid}$ changes from being slightly lower than that of the mantle in Nicaragua to slightly higher in Guatemala. The range in $\delta^{18}O_{Ol}$ values is the same as observed in the South Cascades but the geographic extension is much larger. Extremely elevated $\delta^{18}O_{Ol}$ values for the Kluychevskoy volcano were measured by Dorendorf et al. (2000) and Auer et al. (2009). The latter study advocated that fluxing with a melt rather than fluid in addition to a pre-enriched mantle wedge is required to explain record-high $\delta^{18}O_{ol}$ of up to 7.6‰. We thus favor a melt-mediated transfer of oxygen from the slab to the mantle wedge, and conclude that mantle fluxing by purely hydrous fluids is a less likely mechanism to explain the observed elevated $\delta^{18}O$ subduction signatures. Overall, direct fluid fluxing conditions satisfy the Mt. Shasta BA and PMA $\delta^{18}O_{melt}$ values based on available knowledge of

the fluid proportions and the degree of mantle melting. However, as discussed in the section "*Genesis of HAOT and geodynamic models that can explain their diverse* $\delta^{18}O$ *values*" below, the South Cascades model has to explain across-arc variations observed in both "dry" HAOT and "wet" BA–PMA magma compositions, and we consider the consequences of long-term metasomatic fluid fluxing, particularly in the forearc.

The influence of fracture zone subduction

The additional feature that can explain both high-$\delta^{18}O_{melt}$ and high magmatic production rates in Mt. Shasta is the fact that the South Cascades segment is sandwiched by the projection of the subducting Blanco Fracture zone to the North and the Medocino Fracture zone to the South (Fig. 1). The subduction of such fracture zones could have various implications: (1) A high amount of water input in the subduction zone, as expected by high primary water content measured in melt inclusions (4–6 wt%, Anderson 1974a, b; Ruscitto et al. 2010a, b, with maximum of up to 5.6 wt% in "restored" inclusions based on Anderson's 1974 data but uncorrected for post entrapment crystallization). Indeed, the accumulation of hydrated sediments and the extended exposure surface of the hydrated oceanic crust in the fracture zone lead to an unusual amount of fluids being available during subduction of the fracture zone. (2) Relatively high O-, Li-, Sr-, and Pb-isotope and La/Sm, Ba/Ce, Ba/Nb, Sr/Y ratios in high-Mg magmas due to the mantle source interaction with subduction fluids locally realized from an unusual accumulation of sediments and extended exposure of oceanic crust to low-temperature hydration. (3) Local increase in magma production (related to the high amount of water available), supported by the fact that Mt. Shasta is the largest stratovolcano of the Cascadia arc. Therefore, the subduction of this fracture zone could explain the high $\delta^{18}O_{Ol}$ values measured in Mt. Shasta lavas and thus support the flux melting model (Grove et al. 2002) that needs a large amount of fluids to be released during subduction. Furthermore, a gradual increase of the slab-derived fluid flux from the North to the South Cascades explains the trace element and radiogenic isotope composition change along the volcanic arc (Bacon et al. 1997; Schmidt et al. 2008).

Slab dehydration and δ^7Li *-*$\delta^{18}O$ *isotope systematics across the Cascade arc*

Figure 5 illustrates the across-arc decrease of $\delta^{18}O$ in HAOTs from Mt. Shasta to Medicine Lake. The observed trend indicates that HAOT lavas have progressively lower $\delta^{18}O_{melt}$ as they erupt further from the trench. However, BAs retain constant and relatively high $\delta^{18}O_{melt}$ values in both volcanoes. During magmatic processes, oxygen is a major element whose isotopic balance is primarily controlled by the rock while another stable isotope system, lithium, has smaller abundance and greater affinity for fluids. We compare our oxygen isotope results with those of Magna et al. (2006) who observed a significant (3–4‰) across-arc decrease in lithium isotope compositions (Fig. 5) between BAs and PMAs from Mt. Shasta ($\delta^7Li = 5.1$‰ average in BA) to Medicine Lake ($\delta^7Li = 1.6$‰ average in BA), which they attributed to isotope distillation during progressive slab dehydration.

The Fig. 8 presents isotopic variations in both systems and suggests that the composition of the fluids released during slab dehydration changes as the slab descends deeper into the mantle. Dehydration of deeper slab portions leads to lower δ^7Li and $\delta^{18}O$ values in fluids, similar to processes controlled by Rayleigh distillation, and this process affects isotopes of the trace element lithium more than oxygen. Other traces of subduction fluids, such as high Sr/Y (Fig. 5) also suggest differences across the arc. Overall, the Li-isotopes complement our conclusion derived from the oxygen isotopes and indicate that mantle sources beneath Mt. Shasta and Medicine Lake have been affected by fluids with different compositions.

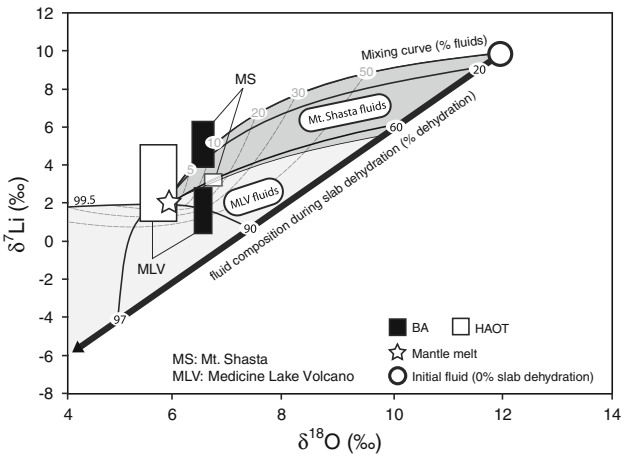

Fig. 8 $\delta^{18}O$ versus δ^7Li composition of the fluids released from the dehydrating subducted slab (*black arrow* with slab dehydration in %). Curves show the mix between mantle-derived melts and fluids (*numbers on curves* correspond to % of fluid). The initial fluid composition ($\delta^7Li = 10$‰ and $\delta^{18}O = 12$‰) corresponds to the composition of the upper part of the slab (e.g., Muehlenbachs 1986; Leeman et al. 2004, and references therein). During slab dehydration, the evolving fluid composition from a finite slab volume was calculated using Rayleigh distillation and fractionation coefficients of 4 and 2‰ for δ^7Li and $\delta^{18}O$, respectively, and Li fluid-slab partition coefficient of $K_D = 2$ (e.g., Leeman et al. 2004). Note that the dehydration of progressively deeper parts of the slab is expected to have the same isotopic effect. The major element composition of the fluid is the same as the water-rich fluid discussed in Fig. 7. δ^7Li_{WR} (whole-rock analyses) are from Magna et al. (2006). Notice that this process may explain the fact that both oxygen and Li isotopic ratios decrease with the increasing distance from the trench (Fig. 5)

Genesis of HAOT and geodynamic models that can explain their diverse $\delta^{18}O$ values

In the previous section, we advocated that the hydrous high-δ^{18}O BAs from Mt. Shasta and Medicine Lake could be generated in direct fluid-induced melting conditions within the current subduction configuration, but the question remains as to how anhydrous and even higher δ^{18}O HAOTs in the vicinity of Mt. Shasta are generated. Furthermore, at Medicine Lake, although the "dry" HAOT's δ^{18}O values are closer to typical mantle-derived melt values (or slightly lower), they are significantly lower than the "hydrous" BA (Fig. 5). HAOTs are normally interpreted to be derived from 6 to 10% partial melting of spinel peridotite in shallow mantle, at depths of ~36 and ~66 km beneath Mt. Shasta and Medicine Lake volcano, respectively, (Elkins-Tanton et al. 2001) under nearly anhydrous conditions (Baker et al. 1994; Grove et al. 2002). As a consequence, HAOTs are good representations of the δ^{18}O value for the shallow mantle beneath the South Cascades.

The trace element spidergram patterns of all HAOT at Medicine Lake and Mt. Shasta show small arc-like enrichments in large ion lithophile elements and depletions in high field strength elements (Bacon et al. 1997; Grove et al. 2002). This implies that the HAOT mantle source has been affected by a subduction component, either during the present day Cascade subduction or sometime in the past.

One possible scenario is that the HAOT lavas in the Mt. Shasta and Medicine Lake regions sample previously subduction-enriched mantle. If so, the present day shallow mantle in the South Cascades has progressively lower δ^{18}O values from west to east (Fig. 5). We suggest that this variation reflects the part of a mantle wedge relic affected sometime in the past by progressively less ^{18}O-enriched fluids, released during dehydration of the contemporaneous subducted slab. Indeed, in the slab dehydration model that we advocate on Fig. 7, the progressively deeper portions of the slab experience dehydration as subduction proceeds. As discussed above, and in line with Schmidt and Poli (1998), slab dehydration beneath the mantle wedge in the South Cascades occurs at high temperatures (>400°C), where subduction $\delta^{18}O_{fluid}$ values approach those of the dehydrating rock. As the δ^{18}O values in the subducted slab decrease from 15 to 0‰ with depth (Fig. 6), the released fluids that interact with the mantle wedge should show identical δ^{18}O range during the subduction process if progressively deeper and deeper parts of the slab are dehydrated.

Questions remain on what particular geodynamic mechanism is responsible for bringing ancient high and low $\delta^{18}O_{fluid}$ signatures into the shallow mantle under the Mt Shasta and Medicine Lake area. We suggest that the model of Zandt and Humphreys (2008), who inferred a mantle flow through the slab window beneath the South Cascades, would fit our geochemical constraints in which the ancient forearc is incorporated into the present subduction configuration. In this process, subduction fluid signature was integrated over millions of years to the ancient forearc mantle peridotite, which is nowadays the source of the HAOT's. This slab edge effect on geochemical signatures (including the δ^{18}O) has been described in other arcs and for explanation of the Central Kamchatka depression in particular (Portnyagin et al. 2007). Other processes that can expose previously fluxed high-δ^{18}O forearc mantle include the subduction outboard jump (e.g., Auer et al. 2009), a conclusion that we favor for magmatism in Kluchevskoy and the Central Kamchatka depression.

High-$\delta^{18}O$ magmas in the southern Cascades and worldwide

As the worldwide dataset for precise δ^{18}O investigations of island arcs grows, the evidence for the presence of very high-δ^{18}O olivine crystals (much higher than the $\delta^{18}O_{Ol}$ mantle value of 5.1 ± 0.2‰) found in mantle-derived magmas grows (Fig. 9). This is characteristic for the southern segment of the Cascade arc, and several other volcanoes. Elevated δ^{18}O values of more than 1‰ have been measured in Mt Rainier, Mt. Lassen, and Mt St Helens lavas of more evolved compositions (Bindeman et al. 2005; Feeley et al. 2008, our unpublished data) relative to the mantle-derived magma differentiation trend. These results permit interpretations involving contamination by high-δ^{18}O crustal material. However, the example of Mt. Shasta shows that highly forsteritic olivine can have high-δ^{18}O and therefore the mantle source itself can be enriched in ^{18}O.

Worldwide, high δ^{18}O values have been measured in olivine crystals from high-Mg lavas (Fig. 9). $\delta^{18}O_{Ol}$ values of more than 6.0‰ and correlated to HFSE (sediment signature) characterize many primitive basalts from the Mexican volcanic zone (Johnson et al. 2009). This oxygen isotope signature is inferred as coming mostly from high-δ^{18}O (9‰) sediment melt. Portnyagin et al. (2007) and Auer et al. (2009) linked high-$\delta^{18}O_{Ol}$ values of up to 7.6‰ in Central Kamchatka Depression with peridotite fluxed by high-δ^{18}O hydrous melt coupled with a subduction roll-back, which exposes to partial melting conditions the highly metasomatized forearc mantle. Additionally, the Central American volcanic arc displays slightly elevated to depleted $\delta^{18}O_{Ol}$ values (from 5.7 to 4.6 ‰), which Eiler et al. (2005) have explained by fluxing of laterally variable δ^{18}O fluid and melt through the mantle wedge.

From a mass balance standpoint, the extreme $\delta^{18}O_{Ol}$ values of more than 6–6.5‰ that we report for Kamchatka

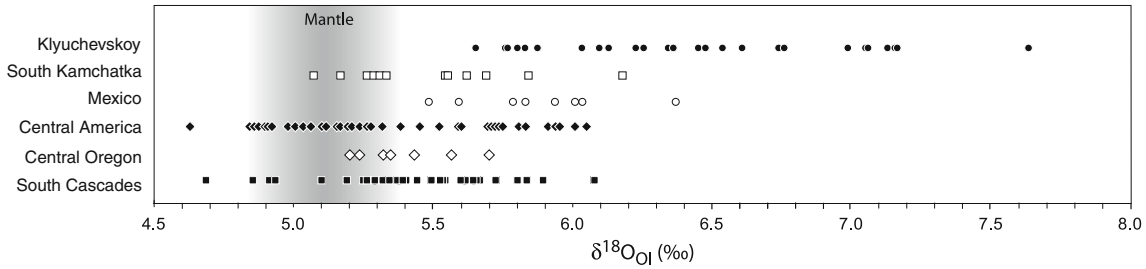

Fig. 9 Oxygen isotope composition of olivine crystals from high-Mg lavas from the South Cascades (this study; see Fig. 3 for more details), compared with the recently measured high-$\delta^{18}O$ olivine signature in other volcanic arc series: the Klyuchevskoy volcano (Auer et al. 2009), South Kamchatka (Portnyagin and Bindeman, unpublished), Mexico (Johnson et al. 2009), Central America (Eiler et al. 2005), and Central Oregon (Ruscitto et al. 2010a, b)

and Mt Shasta cannot be simply attributed to a hydrous subduction fluid interacting with a "normal" $\delta^{18}O$ mantle wedge. Rather, we suggest that the elevated $\delta^{18}O$ signature comes mostly from a ^{18}O pre-enriched mantle wedge through which a moderately high $\delta^{18}O$ hydrous melts or solute-rich fluids have been fluxed. In such a case, the pre-enriched wedge component is hypothesized to be an older forearc mantle with which high-$\delta^{18}O$ fluids have isotopically reacted, without melting, during a prolonged past history (i.e., metasomatic model described above and in Fig. 7). This leads to the long-term ^{18}O enrichment of mantle wedge parts. In the case of Mt Shasta and Medicine Lake volcanoes, this pre-enriched wedge is sampled predominantly by shallow-forming HAOT magmas.

In this study, we have shown that accumulation of ^{18}O is possible in the lithospheric mantle and can lead to high $\delta^{18}O$ values in the most primitive convergent zone magmas. Combined with the "supracrustal" $\delta^{18}O$ signature, acquired by rising magmas in the upper crust, the suggested ^{18}O enrichment of the mantle source could help to explain the frequently observed high $\delta^{18}O$ values of orogenic belts and batholiths.

Acknowledgment This work was supported by the NSF grants EAR-CAREER-0844772 and EAR0537872 to Ilya Bindeman, the NSF grant EAR-0538179 to Timothy L. Grove, and the 'Lavoisier' grant to Erwan Martin. We thank Jim Palandri for his help in the stable isotope laboratory, John Donovan for microprobe analyses assistance, A.T. Anderson for supplying the original samples from his study, Dan Ruscitto and Paul Wallace for discussions and Kathryn Watts, Peter Tollan, Magali Bonifacie, and Lucy Whiteley for proofreading this manuscript.

References

Adami LH, Hildreth W, Donnelly-Nolan JM (1996) Oxygen isotope analyses of 166 rocks samples from Medicine Lake Volcano, California. Open-File report 86-541, US Geol Surv

Anderson AT (1973) The before-eruption water content of some high-alumina magmas. Bull Volcanol 37:243–267

Anderson AT (1974a) Chlorine, sulfur and water in magmas and oceans. Geol Soc Am Bull 85:1485–1492

Anderson AT (1974b) Evidence for a picritic, volatile-rich magma, beneath Mt. Shasta, California. J Petrol 15:243–267

Anderson AT (1976) Magma mixing: petrological process, volcanological tool. J Volcanol Geotherm Res 1:3–33

Anderson AT (1979) Water in some hyperstenic magmas. J Geol 87:509–531

Auer S, Bindeman IN, Wallace P, Ponomareva VV, Portnyagin M (2009) The Origin of hydrous, high-$\delta^{18}O$ voluminous volcanism: diverse oxygen isotope values and high magmatic water contents within the volcanic record of Klyuchevskoy Volcano, Kamchatka, Russia. Contrib Mineral Petrol 157:209–230

Bacon CR, Bruggman PE, Christiansen RL, Clynne MA, Donnelly-Nolan JM, Hildreth W (1997) Primitive magmas at five cascade volcanic fields: melts from hot, heterogeneous sub-arc mantle. Can Mineral 35:297–423

Baker MB, Grove TL, Kinzler RJ, Donnelly-Nolan JM, Wandless GA (1991) Origin of compositional zonation (High-Alumina basalt to basaltic andesite) in the Giant Crater Lava Field, Medicine Lake Volcano, Northern California. J Geophys Res 96:21819–21842

Baker MB, Grove TL, Price RC (1994) Primitive basalts and andesites from the Mt. Shasta region, N. California: products of varying melt fraction and water content. Contrib Mineral Petrol 118:111–129

Barr J, Grove TL, Elkins-Tanton LT (2007) High-magnesian andesite from Mount Shasta: a product of magma mixing and contamination, not a primitive melt: comment and reply. Geology doi: 10.1130/G24058C.1, e147

Benz HM, Zandt G, Oppenheimer DH (1992) Lithospheric structure of Nothern California from teleseismic images of the upper mantle. J Geophys Res 97:4791–4807

Bindeman IN (2008) Oxygen isotopes in mantle and crustal magmas as revealed by single crystal analysis. Rev Mineral Geochem 69:445–478

Bindeman IN, Ponomareva VV, Bailey JC, Valley JW (2004) Volcanic arc of Kamchatka: a province with high-$\delta^{18}O$ magma sources and large-scale $^{18}O/^{16}O$ depletion of the upper crust. Geochim Cosmochim Acta 68:841–865

Bindeman IN, Eiler JM, Yogodzinski GM, Tatsumi Y, Stern CR, Grove TL, Portnyagin M, Hoernle K, Danyushevsky LV (2005) Oxygen isotope evidence for slab melting in modern and ancient subduction zones. Earth Planet Sci Lett 235:480–496

Blakely RJ, Jachens RC, Simpson RW, Couch RW (1985) Tectonic setting of the southern cascade range as interpreted from its magnetic and gravity fields. Geol Soc Am Bull 96:43–48

Ceuleneer G, Le Sueur E (2008) The Trinity ophiolite (California): the strange association of fertile mantle peridotite with ultra-depleted crustal sumulates. Bull Soc Géol Fr 179:503–518

Chiba H, Chacko T, Clayton RN, Goldshmith JR (1989) Oxygen isotope fractionations involving diopside, forsterite, magnetite and calcite; application to geothermometry. Geochim Cosmochim Acta 53:2985–2995

Christiansen RL, Kleinhampl FJ, Blakely RJ, Tuchek ET, Johnson FL, Conyac MD (1977) Ressource appraisal of the Mt. Shasta wilderness study area, Open-File Report 77-250, US Geol Surv

Donnelly-Nolan JM (1998) Abrupt shift in $\delta^{18}O$ values at Medicine Lake volcano (California, USA). Bull Volcanol 59:529–536

Donnelly-Nolan JM, Grove TL, Lamphere MA, Champion DE, Ramsey DW (2008) Eruptive history and tectonic setting of Medicine Lake Volcano, a large rear-arc volcano in the southern Cascades. J Volcanol Geotherm Res 177:313–328

Dorendorf F, Wiechert U, Worner G (2000) Hydrated sub-arc mantle: a source for the Klyuchevskoy volcano, Kamchatka/Russia. Earth Planet Sci Lett 175:69–86

Eiler JM (2001) Oxygen isotope variations of basaltic lavas and upper mantle rocks. In: Walley JW, Cole DR (eds) Reviews in Mineralogy and Geochemistry. The Mineralogical Soc Am, Washington

Eiler JM, Crawford A, Elliot T, Farley KA, Valley JW, Stolper EM (2000) Oxygen isotope geochemistry of oceanic-arc lavas. J Petrol 41:229–256

Eiler JM, Carr M, Reagan M, Stolper E (2005) Oxygen isotope constraints on the sources of Central American arc lavas. Geochim Geophys Gesystems 6:Q07007, doi:10.1029/2004GC000804

Elkins-Tanton LT, Grove TL, Donnelly-Nolan JM (2001) Hot, shallow mantle melting under the Cascades volcanic arc. Geology 29:631–634

Feeley TC, Clynne MA, Winer GC, Grice WA (2008) Oxygen isotope geochemistry of the Lassen volcanic center, Califronia: resolving crustal and mantle contributions to arc magmatism. J Petrol 49:971–997

Fuis GS, Zucca JJ, Mooney WD, Milkereit B (1987) A geologic interpretation of seismic-reflection results in northern California. Geol Soc Am Bull 98:53–65

Gill JB (1981) Orogenic andesite and plate tectonics. Springer, New York, p 390

Goodfellow WD, Grapes K, Cameron B, Franklin JM (1993) Hydrothermal alteration associated with massive sulfide deposits, Middle Valley, northern Juan de Fuca Ridge. Can Mineral 31:1025–1060

Gregory RT, Taylor HP (1981) An oxygen isotope profile in a section of the Cretaceous oceanic crust, Samail ophiolite, Oman: evidence for $\delta^{18}O$ buffering of the oceans by deep (>5 km) seawater-hydrothermal circulation at mid-ocean ridges. J Geophys Res 86:2737–2755

Grove TL, Parman SW, Bowring SA, Price RC, Baker MB (2002) The role of en H_2O-rich fluid component in the generation of primitive basaltic andesites and andesites from the Mt. Shasta region, N California. Contrib Mineral Petrol 142:375–396

Grove TL, Baker MB, Price RC, Parman SW, Elkins-Tanton LT, Chatterjee N, Müntener O (2005) Magnesian andesite and dacite lavas from Mt. Shasta; northern California: products of fractional crystallization of H_2O-rich mantle melts. Contrib Mineral Petrol 148:542–565

Grove TL, Chatterjee N, Parman SW, Médard E (2006) The influence of H_2O on mantle wedge melting. Earth Planet Sci Lett 249:74–89

Harris RA, Iyer HM, Dawson PB (1991) Imaging the Juan de Fuca plate beneath southern Oregon using teleseismic P wave residuals. J Geophys Res 96:19879–19889

Heyworth Z, Turner S, Schaefer B, Wood B, George R, Berlo K, Cunningham H, Price R, Cook C, Gamble J (2007) ^{238}U–^{230}Th–^{226}Ra–^{210}Pb constraints on the genesis of high-Mg andesites at White Island, New Zealand. Chem Geol 243:105–121

Hirose K (1997) Melting experiments on lherzolite KLB-1 under hydrous conditions and generation of high-magnesian andesite melts. Geology 25:42–44

Hoefs J (2005) Stable isotope geochemistry, 5th edn. Springer, Heidelberg

James FD (2002) Geological map of California. California Geol Surv

Johnson E, Wallace P, Delgado Granados H, Manea VC, Kent AJR, Bindeman IN, Donegan CS (2009) The origin of H_2O-rich subduction components beneath the Michoacán-Guanajuato volcanic field, Mexico: insights from magmatic volatile contents, oxygen isotopes, and 2-D thermal models for the subducted slab and mantle wedge. J Petrol (in press)

Kay RW (1978) Aleutian magnesian andesites: melts from subducted Pacific Ocean crust. J Volcanol Geotherm Res 4:117–132

Kay SM, Kay RW, Citron GP (1982) Tectonic controls on tholeiitic and calc-alkaline magmatism in the Aleutian arc. J Geophys Res 87:4051–4072

Kelemen PB (1995) Genesis of high Mg andesites and the continental crust. Contrib Mineral Petrol 120:1–19

Kinzler RJ, Donnelly-Nolan JM, Grove TL (2000) Late Holocene hydrous mafic magmatism at the Paint Por Crater and Callahan flows, Medicine Lake Volcano, N. California and the influence of H_2O in the generation of silicic magmas. Contrib Mineral Petrol 138:1–16

Le Voyer M, Rose-Koga EF, Shimizu N, Grove TL, Schiano P (2010) Two contrasting H_2O-rich components in primary melt inclusions from Mount Shasta. J Petrol 51:1571–1595

Leeman WP, Tonarini S, Chan LH, Borg LE (2004) Boron and lithium isotopic variations in a hot subduction zone-the southern Washington Cascades. Chem Geol 212:101–124

Liakhovitch V, Quick JE, Gregory RT (2005) Hydrogen and oxygen isotope contrains on hydrothermal alteration of the Trinity peridotite, Klamath Mountains, California. Int Geol Rev 47:203–214

Lowenstern JB, Donnelly-Nolan J, Wooden JL, Charlier BLA (2003) Volcanism, plutonism and hydrothermal alteration at Medicine Lake volcano, California. In: Proceedings, twenty-eighth workshop on Geothermal Reservoir Engineering. Stanford University, Stanford, California, 27–29 January, 2003, SGP-TR-173, p 8

Magna T, Wiechert U, Grove TL, Halliday AN (2006) Lithium isotope fractionation in the southern Cascadia subduction zone. Earth Planet Sci Lett 250:428–443

Masi U, O'Neil JR, Kistler RW (1981) Stable isotope systematics in Mesozoic granites of central and nothern California and southwestern Oregon. Contrib Mineral Petrol 76:116–126

Mattey D, Lowry D, Macpherson C (1994) Oxygen isotope composition of mantle peridotite. Earth Planet Sci Lett 128:231–241

Muehlenbachs K (1986) Alteration of the oceanic crust and the ^{18}O history of seawater. In: Valley JW, Taylor HP, O'Neil JR (eds) Stable isotopes in high temperature geological processes. Mineral Soc Am, Washington

Navon O, Stolper EM (1987) Geochemical consequences of melt percolation: the upper mantle as a chromatographic column. J Geol 95:285–307

O'Leary JA, Valley JW, Medaris LJ (1999) Preservation of mantle oxygen isotope ratios in a serpentinized peridotite: Trinity Ophiolitic Complex, California. Geological Society of America Abstracts with programs, Annual Meeting Denver, vol 31, p A164

Peacock SM, Wang K (1999) Seismic consequences of warm versus cool subduction zone metamorphism: examples from north-east and southwest Japan. Science 286:937–939

Portnyagin M, Bindeman IN, Hoernle K, Hauff F (2007) Geochemistry of primitive lavas of the Central Kamchatka depression:

magma generation at the edge of the Pacific Plate. In: Eichelberger J, Izbekov P, Kasahara M, Lees J, Gordeev E (eds), Volcanism and tectonics of the Kamchatka Peninsula and adjacent arcs. American Geophysical Union Monograph Series 172, Washington, pp199–239

Rehkamper M, Hofmann AW (1997) Recycled ocean crust and sediment in Indian Ocean MORB. Earth Planet Sci Lett 147:93–106

Roeder PL, Emslie RF (1970) Olivine-liquid equilibrium. Contrib Mineral Petrol 29:275–289

Ruscitto DM, Wallace PJ, Johnson ER, Kent AJR, Bindeman IN (2010a) Volatile contents of mafic magmas from cinder cones in the Central Oregon High Cascades: implications for magma formation and mantle conditions in a hot arc. doi:10.1016/j.epsl.2010.07.037

Ruscitto DM, Wallace P, Kent A (2010b) Revisiting the compositions and volatile contents of olivine-hosted melt inclusions from the Mount Shasta region: implications for the formation of high-Mg andesites. Contrib Mineral Petrol doi:10.1007/s00410-010-0587-y

Schmidt MW, Poli S (1998) Experimentally based water budgets for dehydrating slabs and consequences for arc magma generation. Earth Planet Sci Lett 163:361–379

Schmidt ME, Grunder AL, Rowe MC (2008) Segmentation of the Cascade Arc as indicated by Sr and Nd isotopic variation among diverse primitive basalts. Earth Planet Sci Lett 266:166–181

Smith IE, Compston W (1982) Strontium isotopes in Cenozoic rocks from southeastern Papua new Guinea. Lithos 15:199–206

Sobolev AV, Hofmann AW, Kuzmin DV, Yaxley GM, Arndt NT, Chung S-L, Danyushevsky VS, Elliot T, Frey FA, Garcia MO, Gurenko AA, Kamenetsky VS, Kerr AC, Krivolutskaya NA, Matvienkov VV, Nikogosian IK, Rocholl A, Sigurdsson IA, Sushchevskaya NM, Teklay M (2007) The amount of recycled crust in sources of mantle-derived melts. Science 316:412–417

Stolper EM, Newman S (1994) The role of water in the petrogenesis of Mariana trough magmas. Earth Planet Sci Lett 121:293–325

Streck MJ, Leeman WP, Chesley J (2007) High-magnesian andesite from Mount Shasta: a product of magma mixing and contamination, not a primitive mantle melt. Geology 35:351–354

Tatsumi Y (1981) Melting experiments on a high-magnesian andesite. Earth Planet Sci Lett 54:357–365

Tatsumi Y (1982) Origin of high-magnesian andesites in the Setouchi volcanic belt, southwest Japan, II. Melting phase relations at high pressures. Earth Planet Sci Lett 60:305–317

Tatsumi Y, Ishizaka K (1982) Origin of high-magnesian andesites in the Setouchi volcanic belt, southwest Japan, I. Petrographical and chemical characteristics. Earth Planet Sci Lett 60:293–304

Tatsumi Y, Hamilton DL, Nesbitt RW (1986) Chemical characteristics of fluid phase released from a subducted lithosphere and origin of arc magmas: evidence from high-pressure experiments and natural rocks. J Volcanol Geotherm Res 29:293–309

Turner S, Handler M, Bindeman IN, Suzuki K (2009) New insights into the origin of O-Hf-Os isotope systematics in arc lavas from Tonga-Kermadec. Chem Geol 5:266, 196–202

Wenner DB, Taylor HPJ (1971) Temperatures of serpentinization of ultramafic rocks based on $^{18}O/^{16}O$ fractionation between coexisting serpentine and magnetite. Contrib Mineral Petrol 32:165–185

Wilson D (1988) Tectonic history of the Juan de Fuca Ridge over the last 40 million years. J Geophys Res 93:11863–11876

Wood BJ, Turner SP (2009) Origin of primitive high-Mg andesite: Constraints from natural examples and experiments, Earth Planet Sci Lett doi:10.1016/j.epsl.2009.03.032

Yogodzinski GM, Volynets ON, Koloskov AV, Seliverstov NI, Matvenkov VV (1994) Magnesian andesites and the subduction component in a strongly calc-alkaline series at Piip volcano, far Western Aleutians. J Petrol 35:163–204

Zandt G, Humphreys E (2008) Toroidal mantle flow through the western U.S. slab window. Geology 36:295–298

Zhao ZF, Zheng YF (2003) Calculation of oxygen isotope fractionation in magmatic rocks. Chem Geol 193:59–80

Zheng Y-F (1993) Calculation of oxygen isotope fractionation in hydroxyl-bearing silicates. Earth Planet Sci Lett 120:247–263

Zucca JJ, Fuis GS, Milkereit B, Mooney WD, Catchings RD (1986) Crustal structure of Northeastern California. J Geophys Res 91:7359–7382